Electrostatic attraction between cationic-anionic assemblies with surface compositional heterogeneities

Y. S. Velichko and M. Olvera de la Cruz*

Department of Materials Science and Engineering,

Northwestern University, IL 60208, USA.

(Dated: February 6, 2008)

Abstract

Electrostatics plays a key role in biomolecular assembly. Oppositely charged biomolecules, for instance, can co-assembled into functional units, such as DNA and histone proteins into nucleosomes and actin-binding protein complexes into cytoskeleton components, at appropriate ionic conditions. These cationic-anionic co-assemblies often have surface charge heterogeneities that result from the delicate balance between electrostatics and packing constraints. Despite their importance, the precise role of surface charge heterogeneities in the organization of cationic-anionic co-assemblies is not well understood. We show here that co-assemblies with charge heterogeneities strongly interact through polarization of the domains. We find that this leads to symmetry breaking, which is important for functional capabilities, and structural changes, which is crucial in the organization of co-assemblies. We determine the range and strength of the attraction as a function of the competition between the steric and hydrophobic constraints and electrostatic interactions.

PACS numbers: 61.46.+w, 64.60.-i, 81.07.-b, 87.68.+z

*Electronic address: m-olvera@northwestern.edu

I. INTRODUCTION

The structure of biomolecular assemblies of cationic and anionic molecules containing hydrophobic groups is controlled by the architecture of the molecules and the intermolecular interactions of the components. The co-assemblies can have spherical, cylindrical or planar symmetries. Oppositely charged lipids, for example, co-assemble into cylindrical micelles[1] or into vesicles[2], while mixtures of cationic and anionic peptide amphiphiles capable of beta sheet formation co-assemble into fibers[3, 4, 5]. The stability of these assemblies is determined by their surface properties, which in turn is the result of the competition between the different type of interactions, similar to proteins[6]. The adsorption of charged lipids onto oppositely charged surfaces[7] is a simple example of planar co-assembly with competing interactions where electrostatics favors homogeneous surface coverage and the lipids hydrophobic tails favor bilayer formation with local excess charge leading to surfaces with charge inhomogeneities. These charge heterogeneities are expected in many cationic-anionic co-assemblies including actin and microtubular associating proteins (MAP) complexes[8], as well as in nucleosomes. Herein we analyze interactions among co-assemblies with surface charge heterogeneities. We show that co-assemblies with homogeneous surfaces interact weakly and induce small changes in the surface heterogeneities of neighboring assemblies suggesting that these co-assemblies have decreased functionality. Meanwhile, co-assemblies with large surface heterogeneities interact strongly and are capable of large structural modifications.

What controls the surface heterogeneities in cationic-anionic co-assemblies? The net incompatibility among chemically different charged components, which in water can be due to different degrees of hydrophobicity, promotes macroscopic segregation of the different components. Meanwhile, electrostatics favors correlated ionic crystal structures. The competition of these interactions result in the formation of surface charge patterns[7, 9, 10, 11] in aqueous interfaces due to the high permittivity of the water. In dense media charges are paired, while in water they can be dissociated. At the interface between a dense media and an aqueous solution, charged patterns of different length scales are possible because the mean permittivity of the two media is sufficiently high. The formation of large domains, which decrease the interface among the components is restricted due to the penalty associated with charge accumulation. Surprisingly this penalty may be overcome in the presence of other as-

semblies, by correlating the oppositely charged domains on the neighboring assemblies. Our computer simulations and theoretical analysis show that the attraction mechanism among co-assemblies is strongly dependent on the degree of compatibility among the co-assembled molecules. Surfaces of co-assembled molecules with large degrees of incompatibility have strong attractions which decay exponentially with separation distance, and the range and strength grow as the degree of incompatibility among the components increases. Compatible co-assembled components have both weak correlated interactions at short distances, and weak dispersion type forces at longer distances similar to the attraction among charged surfaces via their counterions[12, 13, 14].

Formation of surface patterns is not only the result of the interplay of short– and long–range forces. The geometry of the assembly also plays a key role. Cylindrical geometry, where the charged units are confined to the surface of a cylinder, is common in biomolecular assemblies. The appearance of large domains on the surface of cylindrical co-assemblies induce restrictions on the size and symmetry of the domains that affect their physical properties. Such assemblies have attracted much attention as they provide a possible way to create tunable functional biomolecular materials, such as stable vesicles for drug delivery [1, 2] and bio–active fibers [4, 5].

Bundle formation is highly prominent in systems of fibers. Even weak dispersion forces lead to aggregation. In many biological systems the attractions, however, are strong and specific. Here we show that electrostatic interactions are important by modelling cylindrical assemblies of molecules with chemically incompatible oppositely charged head groups exposed onto the surface. This is a coarse grained model for cationic-anionic amphiphile co-assemblies or for self-attracting (hydrophobic) charged particles adsorbed on the surface of oppositely charged fibers such as actin-MAP complexes where the charged proteins effectively change the local properties including local charge density and degree of hydrophobicity [15]. We consider each aggregate as a stable structure, thus constraining the cylindrical geometry and allowing molecules to move only on the surface. The incompatibility among oppositely charged co-assembled molecules per thermal energy K_BT, denoted by χ (expected to be a complex function which includes all the terms opposing mixing of molecules), and the electrostatic interactions determine the surface charge heterogeneities. The study of these interacting assemblies sheds light on the mechanism of non–specific interactions in many biological systems with surface compositional heterogeneities.

The interaction among assemblies with surface compositional heterogeneities have some analogies with the attraction between charged membranes or polyelectrolytes in the solution of neutralizing counterions [13, 16, 17, 18, 19, 20, 21, 22]. However, there is a significant difference. In particular, in case of charged surfaces in the solution of neutralizing counterions, the size of the Wigner crystal cell is determined by the conditions of surface electro-neutrality and $\Lambda \propto \sqrt{Q/(e\sigma)}$, where $e\sigma$ is a surface charge density and Q is the charge of condensed counterions [16]. The fluctuations of condensed ions and structural correlations induce electrostatic attraction. On the other hand, in case of the surfaces with compositional heterogeneities, the size of the Wigner crystal cell is determined by a balance of electrostatic and interfacial energies and $\Lambda \propto \sqrt{\chi/\sigma^2}$. It should be also noticed that the area of the domain determines the effective charge $Q \propto L^2$, while charge of condensed counterion remains the same.

In this paper we study the interaction among cylindrical assemblies with surface compositional heterogenous. We show that the compositional heterogeneities of two interacting cylindrical assemblies are correlated and the size of heterogeneities grows as the assemblies approach each other. This leads to a strong attraction. We show that the effective potential of interaction depends on the degree of surface compositional segregation and the separation distance among assemblies. The range and the strength of the attraction increase as the degree of the net incompatibility of the cationic–anionic components increases.

II. SIMULATION METHOD

We consider each aggregate as a stable structure, thus constraining the cylindrical geometry and allowing molecules to move only on the surface. Within the framework of the primitive model, each aggregates is composed of a stoichiometric mixture of equal number $N_+ = N_-$ of positively and negatively charged units of equal absolute charge $|Q_+| = |Q_-| = 1$ and diameter $a = 1$. The cylindrical assemblies are placed into the box $L_x \times L_y \times L_z$ in the middle of the $YZ-$plane along $z-$axis, where $L_y = L_x + 2R_c + D$. We study the interaction of two parallel cylindrical assemblies of radius R_c and length L_z separated by the distance $2R_c + D$, where D gives the distance between ions on the faced surfaces of the neighboring assemblies. From here, due to the fixed radius R_c, we will use only D to indicate the separation distance.

The surface of each cylinder is filled with units in such a way that all units are placed into the knots of a triangular lattice of period a (Fig. 1) and thus the number surface density is $\sigma = 2/\sqrt{3}a^2$. The short-ranged interaction between units is taken into account via a simplistic discrete van der Waals potential, due to the discreet model. The net degree of compatibility among different components, i.e. positively and negatively charged units, is controlled by Flory–Huggins parameter $\chi = [\varepsilon_{ij} - \frac{1}{2}(\varepsilon_{ii} + \varepsilon_{jj})]/k_BT$, where ε_{ij} represents a pair interaction energy among i and j ions in k_BT units. Compositional incompatibility results in the formation of segregated domains, whose growth is inhibited by electrostatics. We use Debye–Hueckel potential to describe the electrostatic interactions

$$u(r)/k_BT = \ell\frac{e^{-\kappa r}}{r} \tag{1}$$

where $\ell = e^2/4\pi\epsilon_o k_BT$ is Bjerrum length, ϵ_o is the average dielectric constant of the media in units $e^2/4\pi a$ and $\kappa = 4\pi\ell\sum c_i z_i^2$ is the inverse Debye screening length, c_i is the concentration and z_i is the valence of the $i-$th neutralizing counterion in the solution. Taking into account a biological origin of the system, i.e. the large head groups size (~ 10Å) and high average dielectric permittivity of the aqueous solution (~ 80), the Bjerrum length $\ell = 0.2a$ is considered. Due to the assemblies are electroneutral, counterion condensation in not expected in the wide range of temperatures and, thus, we choose Debye length $a/\kappa = 25$.

We report standard canonical Monte Carlo simulations following the Metropolis scheme for various values of $\chi \in [0.5, 12]$, $R_c/a = 2 - 5$, $L_x = L_z$ and $L_z/a = 100$. Simple moves in the phase space are performed by exchange of two randomly chosen particles. Each system is equilibrated during 10^5 MC steps per particle and another 10^5 MC steps are used to perform measurements. The equilibration process is accompanied by a gradual decrease of temperature (temperature annealing) from $T_{max} = 10$ to $T_{min} = 1$.

III. RESULTS

The competition between the net short range repulsion among dissimilar components and the electrostatic penalty associated with the charge accumulation results in the formation of the surface composition heterogeneities. With increase in χ domains size grows, however the electrostatics restrict the possibility of macroscopic segregation. The steric commensurability between the surface charge patterns applies geometrical restrictions on the size

and the symmetry of the domains, and together with the long–range electrostatic interactions induces periodic arrangement of domains of opposite charge, which stabilizes the co-assembled structure in analogy with the Wigner crystals of ions [23]. Figure 2 (a) shows that with increase in χ the normalized energy of the system $U/\chi N$ is decreasing for both, nearby ($D/\sigma = 1$) and separated assemblies. The energy of the nearby assemblies is notably smaller, suggesting a strong attraction among aggregates.

With increase in χ the system undergos transition from the isotropic to segregated phase that is indicated as a broad peak on the heat capacity (Fig. 2 (b)) at χ denoted by χ_1. For nearby assemblies the peak is higher and it is shifted to smaller χ values, suggesting a promotion of the compositional segregation by the assemblies cross–interaction.

A. Theoretical model

Due to complexity of analyzes of cylindrical assemblies, we start by considering two interacting planar surfaces. In the limit of small net incompatibility, the contribution of density fluctuation to the mean free energy can be analyze by means of Random Phase Approximation (RPA) [24]. In the limit of small density fluctuations around an homogenous state of mean density $\bar{\rho}$ equal to the number fraction of positively and negatively charged components $\bar{\rho} = \bar{\rho}_+ = \bar{\rho}_-$. The total free energy F including one loop corrections (OLC) can be obtained from the partition function $Z = e^{-F/k_BT}$. The partition function of the system in terms of the Fourier components of the density ρ_q reads

$$Z = Z_{\rm o} \int \exp\left(-\frac{1}{2V}\sum_{q\neq 0} \rho_q \mathbb{A}_q \rho_q^{\rm T}\right) \prod_{q>0} \frac{d\rho_q}{V} \tag{2}$$

where $Z_{\rm o} = e^{-F_{\rm o}/k_{\rm B}T}$ is zero mode partition function ($q = 0$) with no fluctuation contribution, $\rho_q = (\rho_q^1, \rho_q^2)$, where ρ_q^1 and ρ_q^2 are the Fourier components of the composition fluctuations around the mean value, $\Delta\rho^i(r) = \rho^i(r) - \bar{\rho}$, of cylinder $i = 1, 2$, respectively. $\mathbb{A}$ is the inverse of the density correlation matrix $\mathbb{S}$ with elements $s_{ij}(q) = \left\langle \rho_q^i \rho_{-q}^j \right\rangle$. The diagonal elements $a_{ii}(q)$ of the matrix $\mathbb{A}$ can be estimated according to Cahn–Hilliard free energy of a neutral system [25] with additional gradient (interfacial energy) and electrostatic terms

$$a_{ii}(q) = \frac{1}{\bar{\rho}(1-\bar{\rho})} - 2\chi + \chi\frac{(qa)^2}{2} + 4\sigma u_{ii}(q) \tag{3}$$

where the electrostatic potential

$$u_{ii}(q) = \ell \int \frac{e^{\kappa r}}{r} e^{irq} d\mathbf{r} = \frac{2\pi\ell}{\sqrt{q^2+\kappa^2}}. \tag{4}$$

On the other hand, non–diagonal terms, $a_{ij}(q, D) = 4\sigma u_{ij}(q, D)$, include only the energy of the electrostatic interaction between the separated surfaces

$$\begin{aligned} u_{ij}(q, D) &= \ell \int \frac{e^{\kappa\sqrt{r^2+D^2}}}{\sqrt{r^2+D^2}} e^{irq} d\mathbf{r} \\ &= \frac{2\pi\ell}{\sqrt{q^2+\kappa^2}} e^{-D\sqrt{q^2+\kappa^2}}, \end{aligned} \tag{5}$$

where D is the distance between the surfaces.

B. Domains polarization

In the limit $D \to \infty$, when assemblies do not interact, the competition between electrostatics, $4\sigma u_{ii}(q)$, and interfacial, $\chi(qa)^2/2$, energies result in the formation of favorable density fluctuations of finite wave length q_o^* and appearance of a peak in $s_{11}(q)$ at $q_o^* \simeq (8\pi\ell\sigma/\chi a^2)^{1/3}$(Fig. 3 (a)). Besides, detailed analysis of binary cationic-anionic mixtures restricted on the surface of cylinders [10] and planes [11] reveal many interesting final temperature effects as well as stripe structures along the assembly at lower temperatures.

As one cylinder approaches another, long range electrostatics correlates surface compositional heterogeneities on the neighboring assemblies to minimize the electrostatic energy. In closed vicinity, $D < R_c$, domains of opposite charge are located in front of each other and electrostatic energy of the cross interaction effectively compensates penalty associated with charge accumulation. That results in the polarization or enlargement of the domains. The peak position is shifting in direction of small q values as D decreases (Fig. 3 (a)). In the limit $q_o^* D > 1$, the dependence of the domain size on the distance D among assemblies, calculated form the $\partial s_{11}/\partial q = 0$, has simple approximation

$$q^* \simeq q_o^*(1 - q_o^* D e^{-q_o^* D})^{1/3}. \tag{6}$$

At the same time, the magnitude of the peak $S(q^*)$ is growing with decrease in distance that indicates strengthening of the compositional segregation. Figure 3 (b) shows the OLC critical conditions, obtained from the numerical solution of equation $s_{11}^{-1}(q_o^*) = 0$.

To analyze the domains polarization and compare results of the computer simulation and theory we calculate the static structure factor along the assemblies faced surface

$$S_z(q) = \frac{1}{N_+} \left\langle \left| \sum_{i,j=0}^{N_+} e^{\imath q \cdot \Delta z_{ij}} \right|^2 \right\rangle, \tag{7}$$

where $\Delta z_{ij} = z_i - z_j$ for all ion pairs with equal X and Y components, $x_i = x_j$ and $y_i = y_j$, where $\vec{r}_i = (x_i, y_i, z_i)$ is a cartesian vector. The competition between electrostatic repulsion and interfacial energies results in the formation of most favorable fluctuations of finite wave length $\lambda = 2\pi/q^*$ and the appearance of a peak in $S_z(q)$ at q^*. Figure 4 (b) shows the dependence of q^* versus D for different values of χ. With decrease in the separation distance the q^* is also decreasing, indicating the domains enlargement. For $\chi < \chi^{(1)}$, the q^* always has a final value, while for $\chi > \chi^{(1)}$ for nearby assemblies the domains size becomes in order of the assemblies length (Fig. 4 (a)) indicating a very strong segregation. It is important to underline, that in this case cylindrical geometry results in breaking of symmetry of surface domains, due to $\Lambda \sim R_c$, and then domains grow only along the assembly. Polarization of domains is not only a new and interesting phenomenon that may be used to explain aggregation of different assemblies or biomolecules into bundles. It also affects the effective potential of attraction, due to the dependence of domain size $\Lambda = 2\pi/q^*$ on the separation distance D. Polarization of domains shows another significant difference in the nature of interaction among assemblies with surface compositional heterogeneities and charged membranes or polyelectrolytes in the solution of neutralizing counterions.

C. Electrostatic attraction

The correlation and polarization of surface domains decreases the energy of the system, suggesting the attraction among the assemblies. The strength of the attraction can be calculated from the dependence of energy $U/\chi N$ on the distance D among assemblies, as $\Delta U(D)/N = (U(D) - U_o)/N$, where U_o is the energy of two separated assemblies. At the same time, the energy of two interacting planar assemblies can be analyzed analytically as

$$\Delta E_{2d} = -T^2 \frac{\partial (F/T)}{\partial T}, \tag{8}$$

where F is the OLC free energy (Eq. 2). Figures 5 (a) and (b) show both of the energies for different values of the net incompatibility χ.

In the limit of small net incompatibility, $\chi < \chi_o$, when the surfaces are nearly homogeneous and isotropic, the attraction is originates by cooperative correlations of charge fluctuations leading to a long-ranged power law attraction, D^{-2} [22]. With decrease in the distance D, the density fluctuations are suppressed due to the lateral repulsions among ordered domains. That leads to stronger attraction. On the other hand, with increase in the degree of net incompatibility χ the strength of the attraction is also growing, due to the increasing magnitude of the density fluctuation. However, as we will show later, in the limit of strong incompatibility, $\chi > \chi_o$, we find an unexpected slowly decaying exponential attraction.

In the limit of strong net incompatibility, when surface domains are well pronounced, charged domains correlate themselves to minimize the energy and form one dimensional periodic array. Therefore, the ground state configuration is a pair of two cylindrical assemblies with a charged surface pattern of positive and negative domains in one assembly in front of an oppositely charged domains in the second assembly. In that case, the attraction energy can be approximated as

$$\begin{aligned} \Delta U_{1d}/N &= -\frac{(e\sigma R_c \Lambda)^2}{\epsilon_o} \sum_{m=-\infty}^{\infty} \frac{(-1)^m}{\sqrt{D^2 + (\Lambda m)^2}} \\ &= -\frac{\Lambda (e\sigma R_c)^2}{2\epsilon_o} \sum_{m=1}^{\infty} K_o \left[\pi \frac{Dm}{\Lambda}\right] \{1 - \cos(\pi m)\} \\ &\simeq -\frac{(e\sigma R_c)^2 \Lambda}{\epsilon_o} \sqrt{\frac{\Lambda}{2D}} e^{-\pi \frac{D}{\Lambda}}. \end{aligned} \tag{9}$$

This approximation should work in the limit of thin cylinders, when domain size Λ is large then the radius of the assembly R_c. On the other hand, when $\Lambda < R_c$, cylindrical assemblies can not be considered as one dimensional objects and a planar surface represents another limit. In this case, the attraction energy scales as

$$\Delta U_{2d}/N \simeq -\frac{(e\sigma)^2 \Lambda^3}{\epsilon_o} e^{-2\pi \frac{D}{\Lambda}}. \tag{10}$$

It should be noted here that the domain size Λ is expected to depend on the distance between assemblies.

A possible fitting of the results (Fig. 5 (a)), which sheds some light on the origin of the attraction and also includes the $\chi-$dependence is

$$\Delta U_{fit}^{(d)}/N = U_{(d)}/N - P_1 D^{-P_2}, \tag{11}$$

where d is the space dimensionality, $U_{2d}/N = -E_1 e^{-DE_2}$ and $U_{1d}/N = -E_1 e^{-DE_2}/\sqrt{D}$, and E_1, E_2, P_1 and P_2 are fitting parameters. Taking into account the D dependence of the domain size Λ, we can expect more complex dependence on the separation distance.

Figures 5 (c-f) shows the dependencies of all fitting parameters on χ and compares the corresponding fitting parameters with the parameters we computed analytically. When the system is nearly isotropic, the attraction always includes a short–range (exponential) component and a long-range (power law) component. The short–range term (E_1, E_2) is found in the whole range of χ, suggesting correlations even for small degrees of net incompatibility. Meanwhile the long–range term (P_1, P_2) is found only for $\chi < \chi^{(1)}$, when the system is mostly isotropic. At the point $\chi^{(1)}$ the system undergoes a crossover transition from isotropic to periodic phase and that affects the nature of interaction of the aggregates. For $\chi < \chi^{(1)}$ both parameters E_1 and P_1, those determine the strength of each component of the attraction, exponentially grow with χ, while for $\chi > \chi^{(1)}$, the long–range term diminishes and the short range term changes the dependence on χ. In the strong segregation limit, $\chi > \chi_o$, the long–wavelength density fluctuations and therefore the power law component of the attraction are suppressed by strong domain correlations and the $\chi-$dependence of the exponential term changes with respect to the $\chi < \chi_o$ limit. The multiplicative coefficient E_1 remains nearly constant, while the exponential decay E_2 starts decreasing suggesting a growth in the range of attraction. This is due to the fact that the domain size on the face of the interacting cylinders also grows (Figs. 4 (a)). In the limit of large $\chi > \chi^{(1)}$, since there no long-ranged order in 1D, the long–wavelength density fluctuations are suppressed together with the long–range component of the attraction.

IV. CONCLUSIONS

Compositional heterogeneities and the changes induced by nearby assemblies via correlations and polarization, are key in the design of functional supramolecular assemblies. Correlated domains effectively cancel the electrostatic penalty of each other and amplify compositional segregation. This leads to strong attractions. The cylindrical geometry results in the breaking of the symmetry of the surface patterns, which is important in triggering functional properties. For example, in systems with competing interactions it can explain aggregation of co-assemblies into clusters of different symmetries. The bare length scale

of the charge surface heterogeneity and the degree of polarization determine the symmetry of the bundles of fibers perpendicular to their long axis and unfolds the origin of hexagonal, square or linear (ribbons of fibers) symmetries of supramolecular structures. These effects are of general importance in the organization of biological assemblies. Our results not only explain the mechanism of the attraction between both planar and curved surfaces with charged heterogeneities, but also give insight to the understanding of electrostatic effects in molecular biology[6, 15, 26].

A recent experiment [7] shows the strongly correlated attraction mechanism discussed here among negatively charged surfaces (mica) coated with cationic hydrophobic surfactants (DODA). The surfactants segregate into charged bilayer domains. This leads to a strong attraction among coated parallel surfaces due to the growth of the bilayer charged domains and the correlations between them and the bare mica domains on the neighboring surface.

In summary, we have studied interaction among assemblies with surface compositional heterogeneities. The transition from isotropic to ordered phase leads to formation of charged domains along the cylindrical assembly. The attraction appears as a result of correlations and polarization of charged domains. We show that the interaction among assemblies belongs to the general class of fluctuation–induced forces and includes long– and short–range term. Formation of periodic domains along the cylinder leads to the long–range order of charged domains that suppresses long–wavelength density fluctuations and, thus, long–range component of the attraction. Attraction correlates and polarizes charged domains. Our results reveal the importance of charge heterogeneities in cationic-anionic co-assemblies of complex molecules and suggest a promising strategy for fabrication of assemblies with predictable surface charged patterns for developing functional biomolecular assemblies.

This work is supported by NSF grant numbers DMR-0414446 and DMR-0076097.

[1] E. W. Kaler, K. L. Herrington, A. K. Murthy, and J .A. N. Zasadzinski, *J. Phys. Chem.*, **96**, 6698 (1992).

[2] M. Dubois, B. Deme, T. Gulik-Krzywicki, J. C. Debieu, C. Vautrin, E. Perez and T. Zemb, *Nature*, **411**, 672 (2001).

[3] J. D. Hartgerink, E. Beniash, and S. I. Stupp, Science **294**, 1684 (2001).

[4] K. L. Niece, J. D. Hartgerink, J. J. J. M. Donners, and S. I. Stupp, *JACS*, **125**, 7146-7147 (2003).

[5] G. A. Silva, C. Czeisler, K. L. Niece, E. Beniash, D. A. Harrington, J. A. Kessler, and S. I. Stupp, *Science*, **303**, 1352-1355 (2004).

[6] I. Gitlin, J. D. Carbeck, and G. M. Whitesides, *Angew. Chem. Intern. Ed.* **in press**.

[7] E. E. Meyer, Q. Lin, T. Hassenkam, E. Oroudjev, and J. N. Israelachvili, *PNAS*, **102**, 6839 (2005).

[8] J.X. Tang, P.T. Szymanski, P.A. Janmey, and T. Tao, *European J. of Biochemistry* **247**, 432-440 (1997).

[9] F. J. Solis, S. I. Stupp, and M. Olvera de la Cruz, *J. Chem. Phys.* **122**, 054905 (2005).

[10] Y. S. Velichko, and M. Olvera de la Cruz, *Phys. Rev. E* **72**, 041920 (2005).

[11] S. M. Loverde, Y. S. Velichko, and M. Olvera de la Cruz, J. Chem. Phys **124**, 144702 (2006).

[12] J. Mahanty and B. W. Ninham, in Dispersion Forces. (Academic, New York) (1976).

[13] M. J. Stevens, and M. O. Robbins, *Europhysics Lett.* **12**, 81-86 (1990).

[14] R. Kjellander, T. Akersson, B. Jonsson and S. Marcelja, *J. Chem. Phys.* **97**, 1424-1431 (1992).

[15] L. K. Sanders, C. Guáqueta, T. E. Angelini, J.-W. Lee, S. C. Slimmer, E. Luijten, and G. C. L. Wong, Phys. Rev. Lett., (in press).

[16] I. Rouzina, and V. Bloomfield, *Journal of Physical Chemistry* **100**, 9977-9989 (1996).

[17] J. L. Barrat, and J. F. Joanny, Adv. Chem. Phys., **94**, 1 (1996).

[18] B. Y. Ha, and A. J. Liu, Phys. Rev. E, **58**, 6281 (1998).

[19] J. J. Arenzon, J. F. Stick, and Y. Levin, Eur. Phys. J. B, **12**, 79 (1999).

[20] F. J. Solis, and M. Olvera de la Cruz, *Phys. Rev. E* **60**, 4496-4499 (1999).

[21] J. N. Israelachvili, *Imtermolecular and Surface Forces*, 2-nd edition, Academic Press, New York (1992).

[22] A. Pincus, and S. A. Safran, Europhys. Lett., **42**, 103 (1998); A. W. C. Lau, P. Pincus, D. Levine, and H. A. Fertig, *Phys. Rev. E*, **63**, 051604 (2001).

[23] R.P. Feynman, R.B. Leighton, M. Sands, The Feynman Lectures in Physics (Addison-Wesley, Reading, 1964) sect. II.8.3.

[24] V. Y. Borue, and I. Y. Erukhimovich, Macromolecules, **21**, 3240 (1988).

[25] J. W. Cahn and J. E. Hilliard, J. Chem. Phys., **28**, 258 (1958).

[26] Y. Levin *Physica A* **352**, 43-52 (2005).

FIG. 1: Snapshots of typical configurations of (a) isotropic phase ($\chi = 1.5$) and (b) striped state with defects ($\chi = 10.5$). $D/\sigma = 3$, $R_c/\sigma = 5$ and $L_z/\sigma = 100$.

FIG. 2: The dependence of (a) normalized energy $U/\chi N$ and (b) dimensionless, normalized by N, heat capacity versus χ for different separation distances D.

FIG. 4: (a) Snapshots of typical configurations of surface domains on the faced sites of separated and nearby assemblies for $\chi = 3.0, 6.0$ and 9.0. (b, c) Dependence of $q*$ on the separation distances D calculated in the simulation and numerically ($\partial s_{11}/\partial q = 0$).

FIG. 5: (a) Normalized energy of interaction (points) for two cylindrical assemblies separated by the distance D for different degrees of χ. Solid lines present results of fitting of normalized energy of interaction (Eq. 11), (b) energy of interaction calculated according to Eq. 8, (c-f) fitting parameters E_1, E_2, P_1 and P_2 versus χ.

FIG. 3: (a) The density correlation function $s_{11}(q)$ for different separation distances D and (b) the RPA critical χ_c as a function of D.

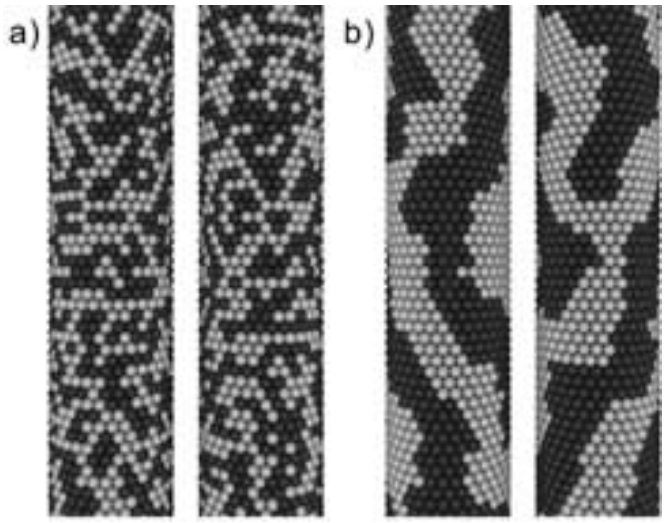

Figure 1

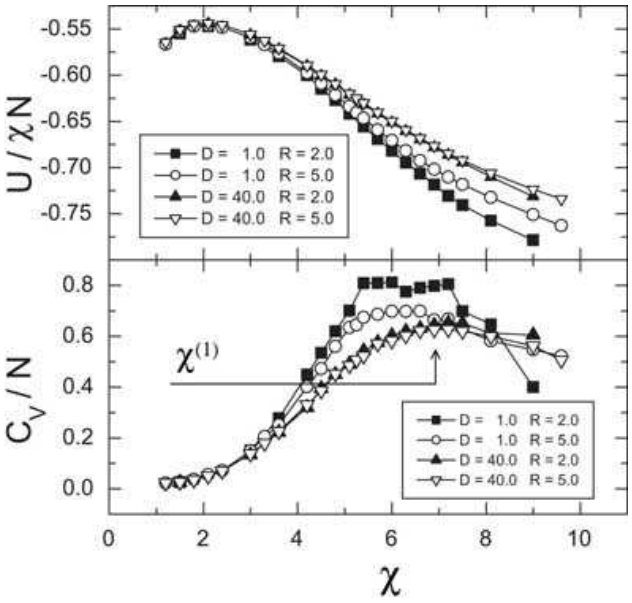
-0.55
-0.60
-0.65
-0.70
-0.75
U / χN
D = 1.0 R = 2.0
D = 1.0 R = 5.0
D = 40.0 R = 2.0
D = 40.0 R = 5.0
0.8
0.6
0.4
0.2
0.0
C_V / N
χ^(1)
D = 1.0 R = 2.0
D = 1.0 R = 5.0
D = 40.0 R = 2.0
D = 40.0 R = 5.0
0
2
4
6
8
10
χ

Figure 2

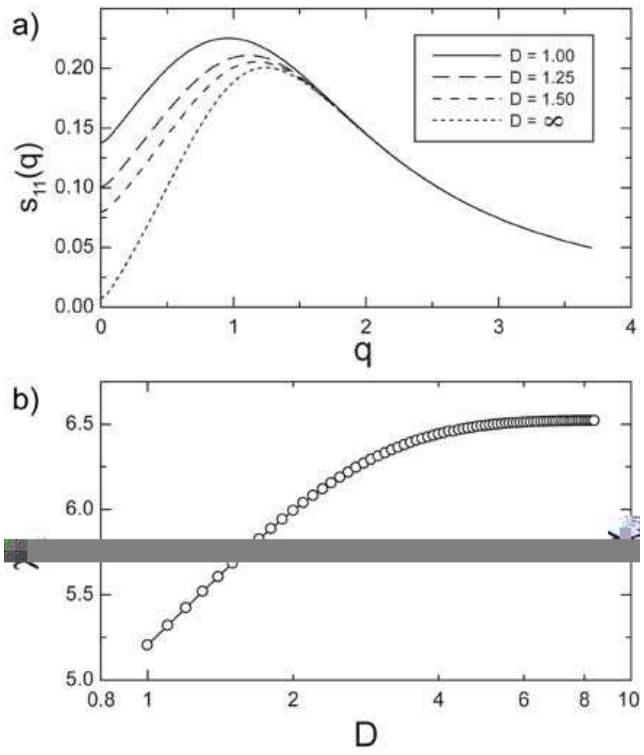

Figure 3

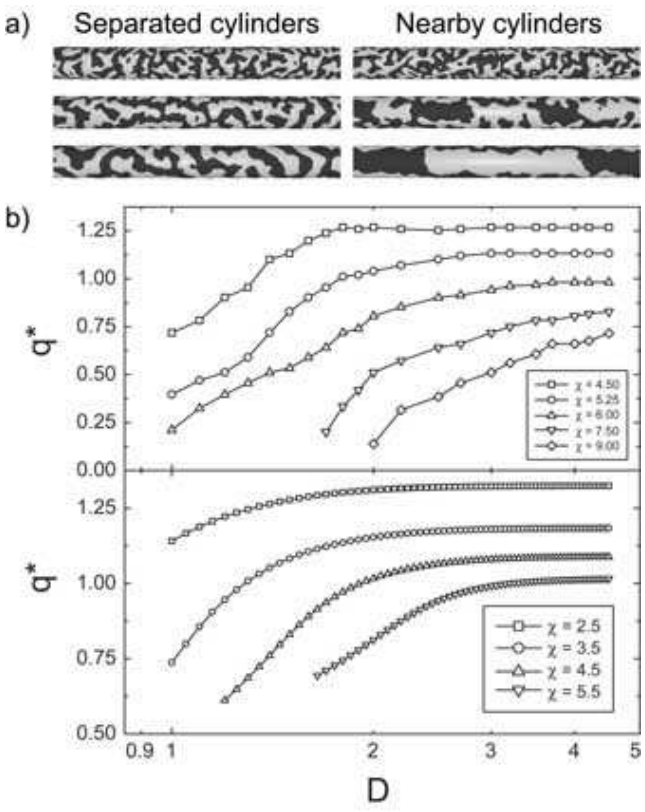
a)
Separated cylinders
Nearby cylinders
b)
q*
1.25
1.00
0.75
0.50
0.25
0.00
χ = 4.50
χ = 5.25
χ = 6.00
χ = 7.50
χ = 9.00
q*
1.25
1.00
0.75
0.50
χ = 2.5
χ = 3.5
χ = 4.5
χ = 5.5
0.9
1
2
3
4
5
D

Figure 4

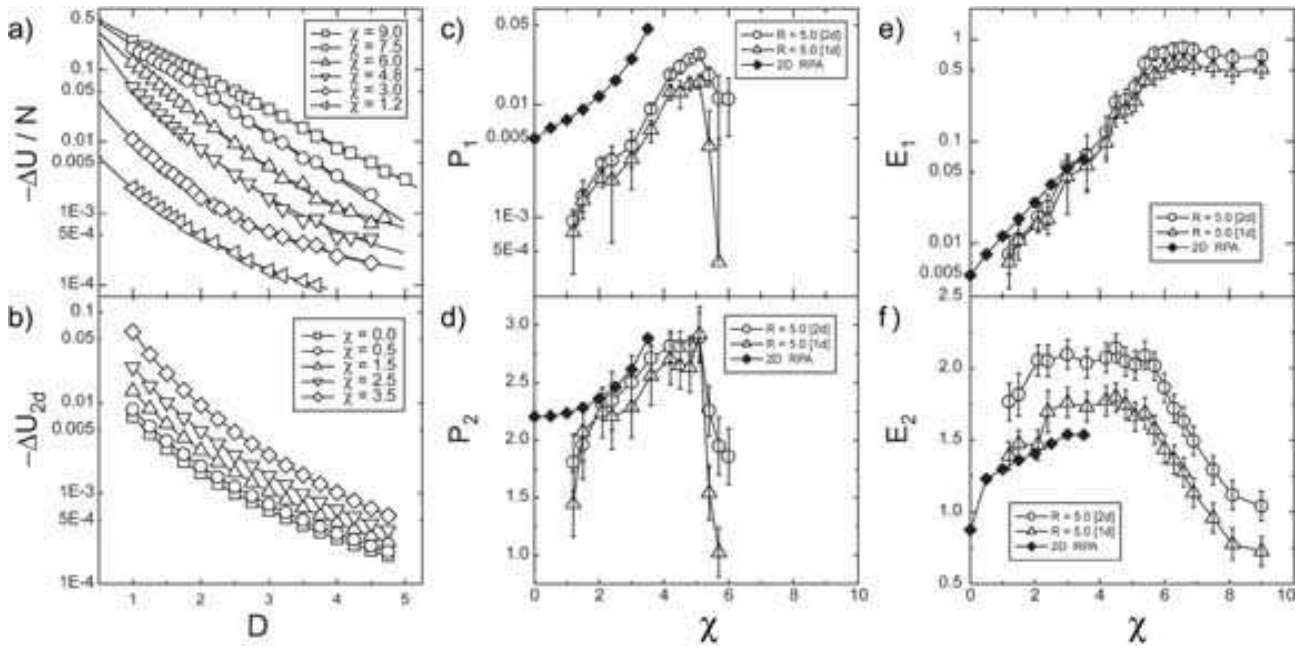
a)
b)
c)
d)
e)
f)
$-\Delta U / N$
$-\Delta U_{2d}$
P_1
P_2
E_1
E_2
D
χ
χ = 9.0
χ = 7.5
χ = 6.0
χ = 4.6
χ = 3.0
χ = 1.2
χ = 0.0
χ = 0.5
χ = 1.5
χ = 2.5
χ = 3.5
R = 5.0 [2d]
R = 5.0 [1d]
2D RPA

Figure 5